T.3: High-power, ultra-short, intense laser pulse driven acceleration and transport of energetic electrons in dense plasma

Tirtha Mandal
Laser Plasma Division
Email: tirtham@rrcat.gov.in

Abstract
A comprehensive investigation on energetic fast/hot electrons (energy: 100s keV - several MeV) generation and transport through dense matter in ultra-short (tens of fs) duration laser pulse interaction with thin (few μm) metal foil targets is presented. Through direct fast electrons as well as indirect x-ray emission measurements, *JxB* mechanism of plasma electrons acceleration applicable in ultra-short intense laser pulse regime has been shown conclusively. The study addresses some important issues for the first time related to fast electrons energy, its dependence on pre-plasma scale length, demonstration of superponderomotive acceleration of electrons and counterintuitive polarization dependence for *JxB* heating. Laser to fast electrons conversion and transport processes were investigated using various x-ray emission measurements. In addition to direct relevance in generation of energetic electrons and x-ray radiation, the study is of significance for proton/ion acceleration from rear of thin foil target, warm dense matter and fusion related aspects.

1. Introduction

The invention of high-power pulsed lasers in last few decades have given us the opportunity to study the plasma in extreme condition similar to astrophysical objects [1,2]. Particularly the invention of mode-locking and chirped pulse amplification (CPA) technique by D. Strickland and G. Mourou [3] made it possible to generate ultrashort pulses of tens of femtosecond (fs) duration with peak laser power from several terawatt (TW) to petawatt (PW) levels. When such laser pulse is focused to a size of few μm using off-axis parabolic mirror, it yields an enormous intensity (I) in the range of ~10^{18}-10^{22} W/cm^2, leading to creation of plasma under extreme conditions. Due to extremely high electric field (Giga to Tera Volt per meter) created at the plasma, electrons and protons are accelerated to very high energy (~ keV to tens of MeV) from the interaction region. The study of energetic electrons generation and transport in dense solid is a subject of research investigation for various potential applications including laser driven fast ignition approach to inertial confinement fusion [4], proton and ion acceleration [5] to tens of MeV energy for practical applications including cancer therapy, creation of high brightness, ultrashort broadband x-ray sources[6] and creation of warm dense matter.

2. Ultra-short, ultra-high intensity laser plasma interaction physics

A schematic of laser matter interaction and subsequent energetic particle generation is shown in Figure T.3.1(a). Laser pulse is focused using suitable optics on thin foil targets. The tiny focal spot (few μm diameter) leads to ultra-high peak laser intensity (>10^{19} W/cm^2) on the target, leading to plasma formation by the foot of the laser pulse. In laser solid (dense plasma) interaction, different laser absorption mechanisms [2] are applicable, viz., resonance absorption, vacuum heating and *JxB* heating[7] for the generation of relativistic fast electrons. The absorption mechanisms are governed by the laser and plasma parameters and are summarized in Figure T.3.1(b). For example, at relativistic laser intensity (I >10^{18} W/cm^2), *JxB* heating is most dominant, as the electrons oscillating along the laser electric field direction get pushed by the *vxB* force along the laser propagation direction. Understanding the laser plasma coupling at such extreme condition is a unique research problem, which leads to generation of energetic electrons in the range 10s of MeV.

Next, fast electrons generated at front surface propagate through overdense medium and encounters complex transport phenomena as shown in Figure T.3.1(c). In cold solids, a strong electric field is generated, which inhibit fast electron penetration in target [2]. Further, huge magnetic field (~MG) is also generated, which tries to pinch the beam. In thin foil targets, the escape of energetic fast electrons from front and rear surfaces creates a strong sheath electric field [8] (~TV/m), which is responsible for accelerating proton. Improvement in electron flux and energy leads to the generation of energetic proton with higher energy. Next, due to the strong sheath fields, fast electrons reflux within the target, known as refluxing [9,10]. Further, this process can result in relatively higher electron energy and temperature [11-13] through 're-acceleration' of electrons by laser pulse. Next, fast electrons while propagating through solid produces bremsstrahlung and x-ray line radiations, which are used as a reliable diagnostic for fast electrons studies. Understanding the transport phenomena in solid will help in improvement of overall beam quality of electrons and proton beams apart from their importance in laser driven fusion approach.

Mostly, for fast electron generation and transport studies, metal targets are used. However, fast electron studies in transparent and dielectric mylar (polyethylene terephthalate) target also attract special attention due to their low electrical conductivity resulting in complex electron transport properties [2]. Further, with such targets, being transparent, Cherenkov radiation imaging can also be used to investigate fast electron transport. However, it has been observed that in insulator mylar target, the fast electron and K_α conversion efficiency is low as compared to metal target due to electric field inhibition inside the target material. Therefore, it is important to explore the techniques for improving the electron flux and energy in mylar target in order to use such targets for fast electron transport studies.

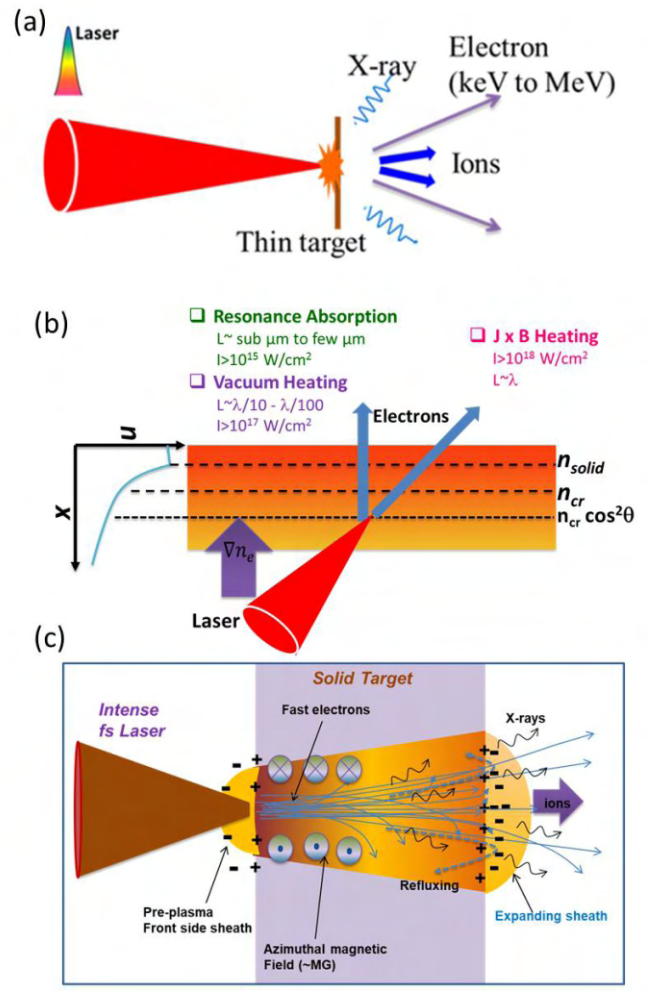

Fig. T.3.1: (a) Schematic of ultra-short ultra-high laser foil interaction and energetic particle generation, (b) different absorption mechanisms for different intensity (I) and pre-plasma density scale length (L) regime, and (c) schematic of fast electron transport through solid density matter.

3. Experimental setup

The schematic of experiment setup for fast electron angular and spectral distribution measurement is shown in Figure T.3.2(a). The ultrashort (~25 fs), high power Ti:sapphire laser (150 TW laser system) was focused using off-axis parabolic mirror to few micrometer focal spot on the thin metal foil target at oblique incidence (10°-60°) yeilding intensity of ~1 - 7x10^{19} W/cm^2. The fast electrons emitting from the interaction region were detected using DRZ setups made up from a combination of Gd_2O_2Si:Tb phosphor screen (trade name: DRZ High) and CCD cameras (14 bit PCO-Pixelfly). Three such setups (DRZ-1, DRZ-2 and DRZ-3) were used to measure the angular distribution over a wide angular range around the laser axis as shown in Figure T.3.2. The phosphor screen was shielded from ions, plasma light and low energy x-rays using Al filter. The average charge of the escaped electrons was estimated from the integrated CCD count using calibration of phosphor. Energy spectrum of the electron beam was measured using magnetic spectrograph. The spectrograph consists of a rectangular dipole magnet (length: 5 cm, pole gap: 5 cm) and a phosphor screen-CCD combination as a detector. The actual optical and mechnaical setup including the large size off-axis parabolic mirror, folding mirror, remotely controlled motorized target positioning system, etc. used inside the experimental chamber are shown in Figure T.3.2(b)

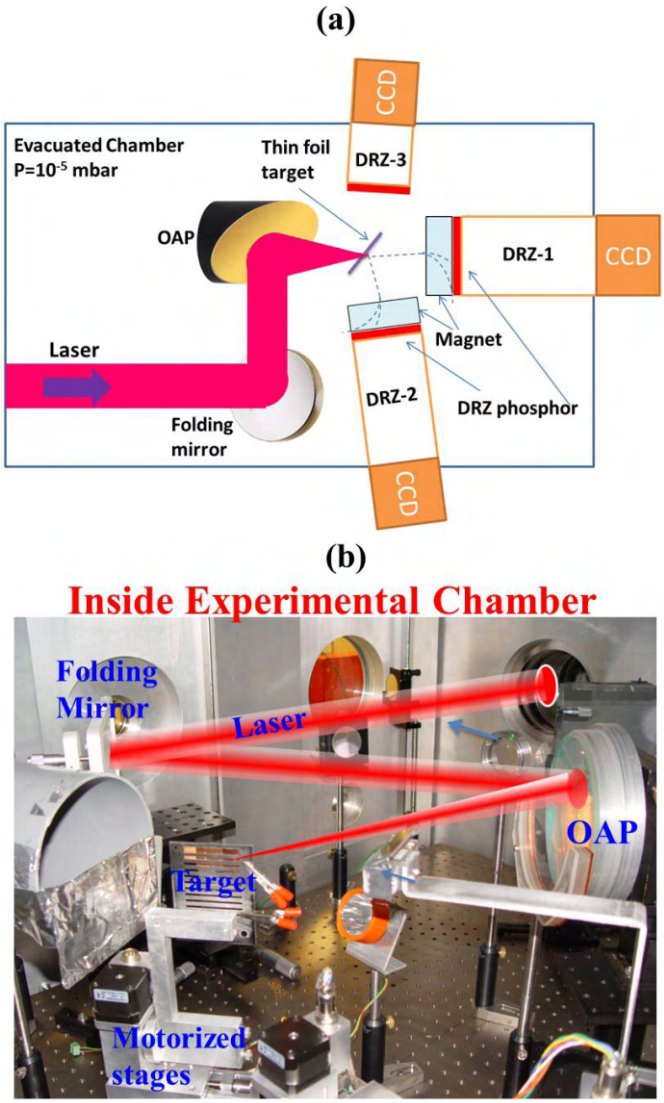

Fig. T.3.2: (a) Schematic for experimental setup for fast electron angular and spectral distribution study. Three phosphor screen-CCD camera setups were placed around the interaction region. For enegy distribution measurement, magnets were placed infront of the phosphor screens and (b) actual optical and mechnical setups inside the experimental chamber containing the off-axis parabolic mirror (OAP), target and motorized stages, etc.

Investigations were performed with peak intensity of ~1 - 7x10^{19} W/cm^2 using 150 TW Ti:sapphire laser system. The peak intensity was achieved by focusing pulse energy of ~0.16 - 2.2 J with duration of ~ 25 fs (FWHM) to small focal spot size of about few μm (FWHM). The amplified spontineous

emission (ASE) intensity contrast at 1 ns prior to fs pulse was measured to be <$2x10^{-10}$. Mostly, thin metal foils of Cu (thicknesses 2 - 100 µm) were used as target. Laser incidence angle with respect to target normal varied from ~10° to ~ 60° during the experiment by rotating the target with respect to laser axis in the incidence plane. The peak laser intensity was varied by three different methods: (i) by reducing the laser pulse energy, (ii) increasing the focal spot size, and (iii) increasing the laser pulse duration during the experiment. Laser polarization was changed from *p*- to *s*- by inserting a half wave plate in the laser beam path after the pulse compressor unit.

3.1. JxB heating and counterintuitive polarization dependence of fast electrons

First, the study of fast electron generation from thin metallic foils in oblique incidence interaction was carried out [14]. The measurements were performed for wide range of parametric variations, viz., laser intensity (~0.8 to $7x10^{19}$ W/cm^2), polarization (*p* and *s*), incidence angle (~20° - 60°), pulse duration (~ 25 fs to ~ 1300 fs), focal spot size (~ 5 µm to ~ 255 µm), pre-plasma scale length and target thickness (~ 2 µm to ~ 100 µm). Energetic electron beams (charge: ~0.3 - 2 nC, maximum energy ~ 1 to ~ 8 MeV for *I* ~ 1 - $7x10^{19}$ W/cm^2) were observed along laser propagation direction as shown in Figure T.3.3. Further, electron beams (charge: ~ 30 - 115 pC, maximum energy ~1 to ~3 MeV for I ~1 - $4x10^{19}$ W/cm^2) in the transverse direction was also observed (Fig. T.3.3(a)). Emission of electrons along laser direction in such high contrast condition indicates clear demonstration of *JxB* mechanism. Electron beam along laser transverse direction indicates the role of laser electric field in electron acceleration along polarization direction. Simultaneous emission of electrons in laser propagation and transverse directions has been observed for the first time due to unique interaction condition.

Energy spectra analysis (Fig. T.3.3(b)) showed that the forward electrons have less temperature (e.g., ~ 0.43 MeV at *I* ~$4x10^{19}$ W/cm^2) than ponderomotive scaling (~1.75 MeV), which is counterintuitive in nature. The reasons were found out to be unique interaction condition occurring at sharp density plasma and energy loss during escaping process at the rear surface [14].

Next, counterintuitive observation of strong polarization dependence of fast electrons was observed, e.g., electron flux reduced to about 4 times and maximum energy reduced from ~3 MeV to ~1 MeV on changing polarization from *p*- to *s*- at *I* ~$4x10^{19}$ W/cm^2 as shown in Figure T.3.3(a) and T.3.3(b). This contrary behaviour suggests role of pre-acceleration of electrons by polarization dependent mechanism in the rising part of the laser pulse [14]. The polarization dependence of electrons vanished in presence of longer scale length pre-plasma.

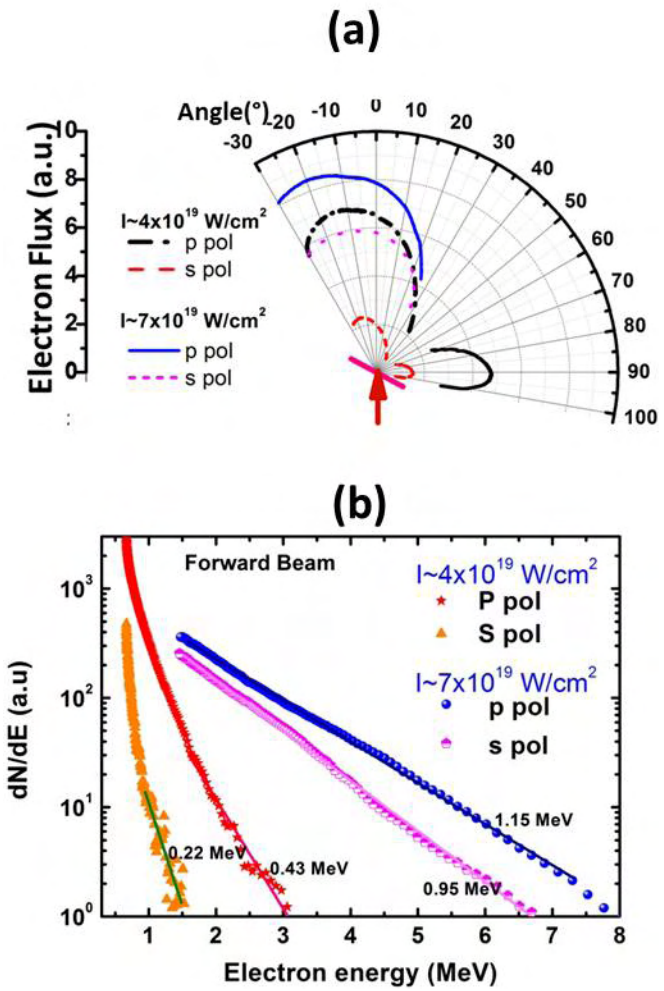

Fig. T.3.3: (a) Spatial profile of fast electrons in forward and transverse directions for p and s polarization and (b) electron energy spectrum at intensities of ~$4x10^{19}$ W/cm^2 and ~$7x10^{19}$ W/cm^2 for both the polarizations.

Further, the refluxing and reacceleration phenomena of electrons was inferred by comparing the flux of escaped electrons as a function of intensity varied by changing laser pulse energy, pulse duration and focal spot size and also from thickness variation study [15]. It was observed that in all methods of changing laser intensity, the overall charge, maximum energy and temperature reduces with decrease in laser intensity. However, the rates of decrement in three methods are different. In case of laser focal spot variation, the decrease rate is slowest whereas for pulse duration variation, the decrease rate is in between of laser pulse energy variation and focal spot variation. The propagation of fast electrons inside target foil and their escaping from targets is strongly affected by refluxing phenomena. Along with this, reacceleration of electrons can also happen, which can result in relatively higher electron energy and temperature. The condition for reacceleration is that the laser pulse duration has to be larger than twice the electron traverse time through the

target foil, so that back reflected electrons can get reaccelerated again by the laser field present at the front surface. The reacceleration of electrons was evident in the observation showing higher temperature electrons in thinner foils. Next, hard x- ray (>22 keV) angular distribution measurement and laser energy absorption measurements were also performed, which corroborates the fast electron experimental results.

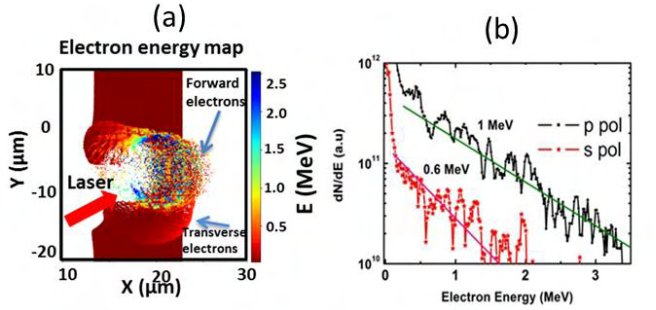

Fig. T.3.4: 2D PIC simulation results: (a) electron energy map clearly showing the forward and transverse electron emission and (b) energy spectra of the forward beam for p- and s-polarization at intensity of $2x10^{19}$ W/cm^2.

2D particle-in-cell (PIC) simulations were also performed to understand the experimental results at intensity of $2x10^{19}$ W/cm^2 as shown in Figure T.3.4. The angular distribution of electrons of different energy is shown in Figure T.3.4(a), which clearly shows the forward accelerated electrons produced from *JxB* mechanism along with the transverse low energy electrons. The strong polarization dependence of forward electrons was also replicated in simulation showing more flux and more energy for *p*- polarization (Fig. T.3.4(b)).

3.2 Superponderomotive acceleration of fast electrons

Fast electron generation in presence of larger pre-plasma scale length was investigated using an additional pre-pulse beam irradiating the target at different delays [15]. More flux and high energy electrons were obtained in longer scale length. The maximum energy (and temperature) increased from ~3 MeV (~0.35 MeV) to ~6.5 MeV (~1 MeV) with introduction of pre-pulse at 0 ns and further up to ~ 16 MeV (~2.86 MeV) for - 4 ns delay before the main pulse. Most importantly, at larger scale length (L/λ>>1, L: scale length and λ: laser wavelength) pre-plasma condition created using pre-pulse at delay of >1 ns, fast electron temperature beyond ponderomotive limit was observed (Fig. T.3.5). The temperature scales with scale length as $T \propto L^{0.59}$ and shows a saturation effect at longer scale length. The overall results indicate a gradual change in absorption mechanism from *JxB* heating at sharp density interaction to stochastic heating at large pre-plasma scale length generating super-ponderomotive electrons through efficient acceleration from the standing wave structure pattern. The experimental results were also verified through PIC simulation, where increase in electron energy with increase in scale length was observed.

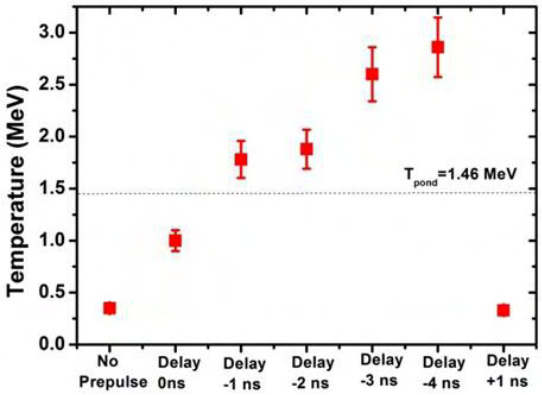

Fig. T.3.5: Fast electron temperature is plotted for different pre-pulse delay from 1-4 ns. Main pulse: energy: 1.2 J, duration: 25 fs, intensity: $3x10^{19}$ W/cm^2. pre-pulse: energy: 150 mJ, 600 ps, $1x10^{13}$ W/cm^2.

4. Investigation of fast electrons using dielectric targets

Next, fast electron study was performed in transparent dielectric and layered dielectric target to investigate the core fast electron transport related issues such as electric field inhibition, sheath field dynamics, etc.

4.1 Probing electric field inhibition using dielectric transport layer

First, we performed the fast electron generation from bare mylar (polyethylene terephthalate) foil and its comparison with metallic Cu foil. Figure T.3.6 shows the electron energy spectrum for bare mylar foil and its comparison with Cu. The maximum energy for mylar extends upto ~0.4 MeV with a fitted electron temperature of ~0.07 MeV. In comparison, for Cu foil (7 μm) has maximum energy of ~1 MeV with temperature of ~0.12 MeV. Therefore, the maximum energy and temperature for bare mylar is ~2.5X and ~1.7X smaller, respectively as compared to Cu foil. Similarly, the total charge of electrons with energy >70 keV for bare mylar was ~6.6 X smaller than the Cu foil. The dominant reason for such reduction of electron charge and energy is found to be the electric field inhibition during electron transport through matter due to dielectric nature of the mylar, which is absent in Cu.

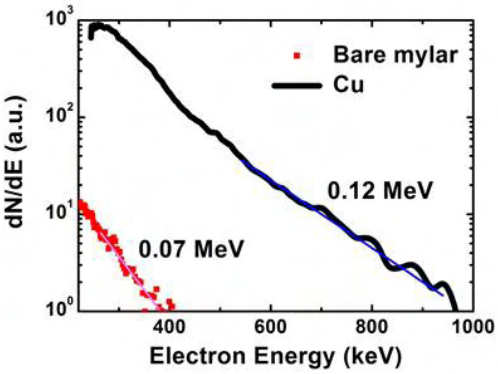

Fig. T.3.6: Energy spectrum of electrons for bare mylar (8 μm) and Cu (7 μm), intensity of ~$1x10^{19}$ W/cm^2, angle of incidence: 30°.

4.2 Improvement in electron energy and probing sheath dynamics using layered dielectric targets

Next, a novel technique was proposed for studying sheath dynamics by creating plasma using metal coating on the front and rear surface of transparent mylar target [16]. The electron flux and energy increased (flux ~1.8 X and energy ~2.5X at I ~1x10^{19} W/cm^2) when a thin (~50 nm) metal (Al) coating was applied in the front of mylar compared to bare mylar as shown in Figure T.3.6. This enhancement is explained from the larger laser absorption in longer pre-plasma in critical density region formed for metal coated mylar. Self-focusing of laser pulse in extended pre-plasma also helps in increase of laser intensity resulting in improvement in electron flux and energy.

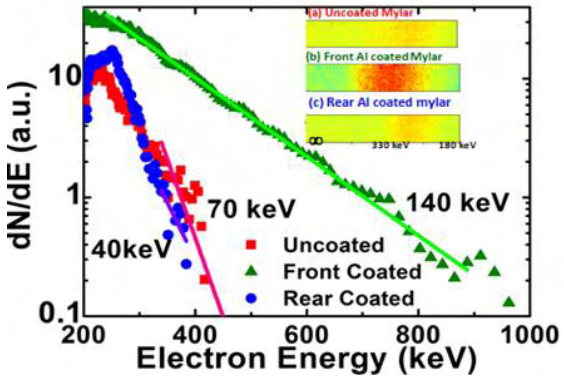

Fig. T.3.7: Fast electron spectrum for uncoated, front Al coated mylar and rear Al coated mylar.

Further, electron flux increased (~1.4 X at I ~1x10^{19} W/cm^2) for rear Al coated mylar but without any change in maximum energy as shown in Figure T.3.7. As the fast electron energy is decided mostly by the front surface pre-plasma condition, the energy was unchanged in case of rear Al coated mylar. However, the enhancement of electron charge is explained by considering the presence of pre-plasma at rear, leading to delay in formation of rear sheath field resulting in larger escaped electron flux. The study brings out important aspects of fast electron generation using a fs laser system by using a layered target design, which could be of interest to control the fast electron generation.

5. Improvement in electron beam properties utilizing grazing incidence interaction

Generally, fast electron generation depends on various laser-solid interaction parameters and broad angular distribution of electrons peaking along laser propagation direction was observed with wide divergence of ~80º - 90º. However, for practical use of such electrons beams, improvement in electron parameters are required particularly the electron beam divergence. It has been found that in the presence of self-induced quasistatic electric and magnetic fields, fast electrons emission direction as well as divergence can be strongly modified. At grazing incidence interaction (incidence angle ~70º), the generation of surface fields and interaction of electrons with the surface field can be enhanced leading to a highly collimated and directional electron beam to be useful for different applications. Further, it is also important to understand the generation and transport of fast electron in the context of hollow re-entrant cone target proposed for the fast ignition experiment as in this case electrons are generated in cone sidewalls at grazing incidence.

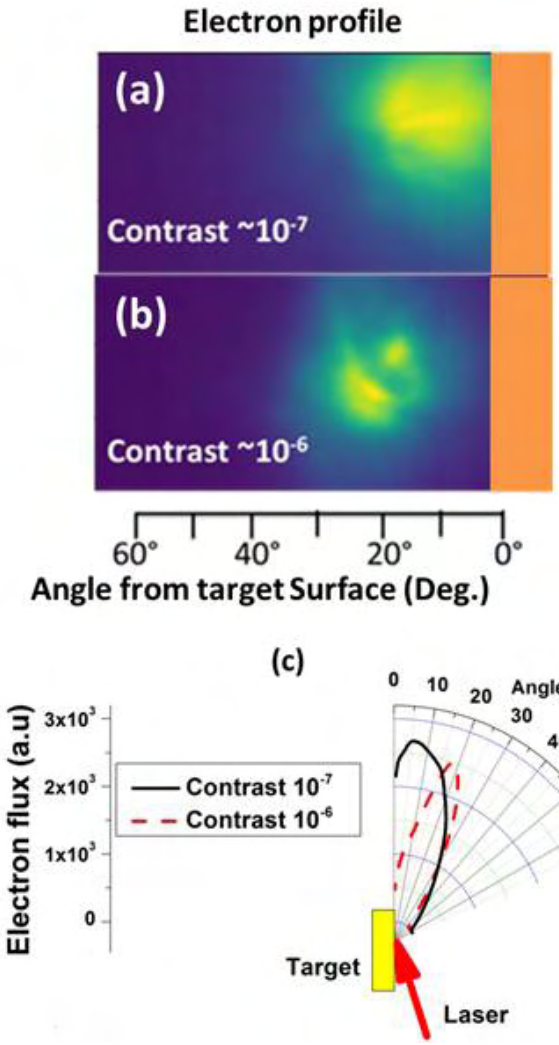

Fig. T.3.8: Typical electron beam profiles as recorded on phosphor screen for (a) contrast of 10^{-7} and (b) contrast of 10^{-6}, and (c) polar plot of electron beam in the incidence plane for the two contrast cases.

First, the grazing incidence interaction study was performed [17] at laser intensity of ~1x10^{18} W/cm^2 as shown in Figure T.3.8. The fast electrons were observed along target surface direction for small pre-plasma scale length at better contrast of ~10^{-7} (Fig. T.3.8(a) and T.3.8(c)). However, with the increased pre-plasma scale length (contrast ~10^{-6}), the collimated (divergence angle ~20^0) fast electron emission was obtained along the specular direction (Fig. T.3.8(b) and T.3.8(c)). The emission direction further moves towards the target normal direction with further increase in pre-plasma scale length. The electron characteristics including emission direction, divergence angle and charge of the fast electron was found to depend strongly on the target material and pulse duration

whereas showed weak dependence on the polarization of laser beam. The electron beam charge was maximum in Si target, which could be attributed to the higher laser absorption depth in the material.

The experimental results were understood considering the role of quasistatic electric and magnetic fields present on the target surface. The 1-D hydrodynamic simulation using HELIOS [18] estimated the scale length of plasma density profiles for different ASE contrast, extent and for different target materials and was useful in understanding the experimental results. The 2D PIC simulation using EPOCH [19] was also run for two different pre-plasma scale lengths of 1 µm and 4 µm, which showed electrons are ejected along the surface direction for smaller pre-plasma scale length.

Next, the grazing incidence study was extended in thin foil target at higher intensity of ~7x10^{19} W/cm^2. Here, we obtained electron beam both along front and rear surface as shown in Figure T.3.9(a) and T.3.9(b). Compared to oblique incidence interaction, the rear electron beam was more inclined towards target surface direction with higher charge (~ 4±0.6 nC) and reduced divergence (~ 65°±5°). On the other hand, the front escaped electrons were highly collimated (~7º) and guided along the target surface direction showing the influence of quasistatic surface fields.

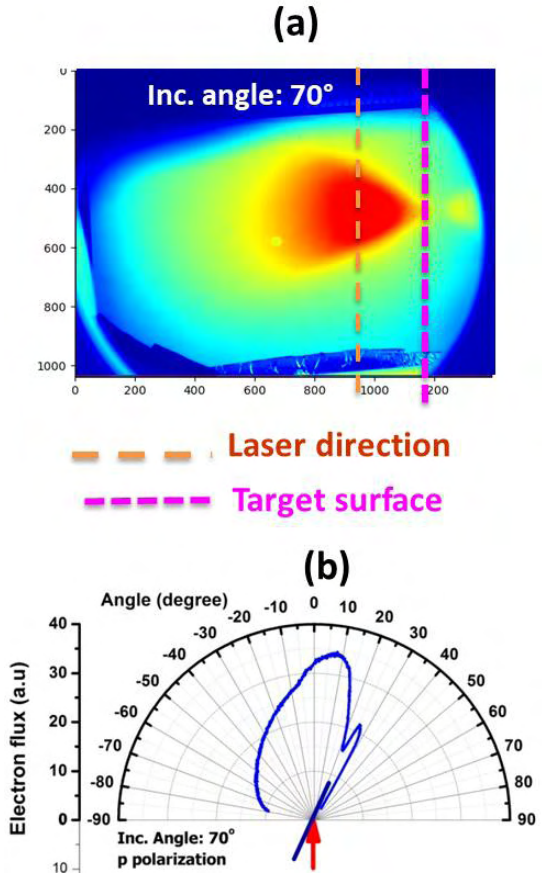

Fig. T.3.9: Electron (a) beam profile and (b) polar plot of fast electrons for 45° and 70° incidence angle.

6. Fast electron transport study through x-rays measurements

By measuring the fast electrons directly, we mostly infer interaction dynamics of escaped electrons. To understand the transport by the confined electrons, x-ray measurements are very important. Some important aspects such as laser to fast electrons conversion efficiency, applicable absorption mechanism, refluxing, reacceleration, etc. can be investigated by measuring flux of x-ray radiation.

High resolution x-ray spectroscopic measurements are generally carried out for investigation of above mentioned aspects. Crystal spectrographs are generally used for the measurement of high resolution x-ray line radiations. Further, the knowledge of x-ray source size is useful for finding the fast electron divergence angle in dense solid. The x-ray source size (akin to the electron source size) measurement can be performed using different techniques such as x-ray shadowgraphy using the knife-edge technique or by monochromatic 2D K_α imaging.

First, 1D imaging [20] of broadband x-ray source size was performed using knife edge shadowgraphy technique. The front as well as rear side source size was measured. Further, the effect of laser intensity, pulse duration and ASE contrast on x-ray source size was studied to investigate the probable role of these laser parameters on electron divergence inside target material. Fast electron divergence was measured using specific layered target consisting a propagation layer and a tracer layer. A half divergence angle of ~37°±10º was estimated by measuring the rear side x-ray source sizes with different thicknesses at a laser intensity of ~1.3×10^{18} W/cm^2.

Next, 2D imaging of monochromatic Cu K_α source from target front and rear surface was performed using a spherically bent quartz crystal spectrograph at a laser intensity of 7x10^{19} W/cm^2. High resolution spherically bent quartz crystal spectrograph was used to image Cu $K_{\alpha 1}$ (8.047 KeV) source size at the target front and rear surface. The schematic of the setup is shown in Figure T.3.10(a). A spherically bent quartz crystal and x-ray CCD camera was used in the spectrograph in an appropriate geometry with a magnification of ~8.1. For front side imaging, incidence angle was kept at ~30°, such that the crystal faces the target front surface and interaction region in the normal direction and therefore will provide near circular x-ray images. For rear side imaging, the target was rotated in clockwise direction keeping the crystal position fixed such that the crystal faces the rear surface. However, the incidence angle was limited to ~70° in this case. Front side source size was calculated to be ~38 ± 2 µm (Fig. T.3.10(b)) whereas the rear side source size was estimated be ~47 ± 2 µm and 58 ± 4 µm for Cu 7 µm and Cu 25 µm foil, respectively. A fast electron half divergence angle of ~17° inside target material was calculated from the fitting of rear side source sizes. Such small divergence indicates the acting role of self-generated mega gauss magnetic fields on collimating fast electrons at high laser intensity.

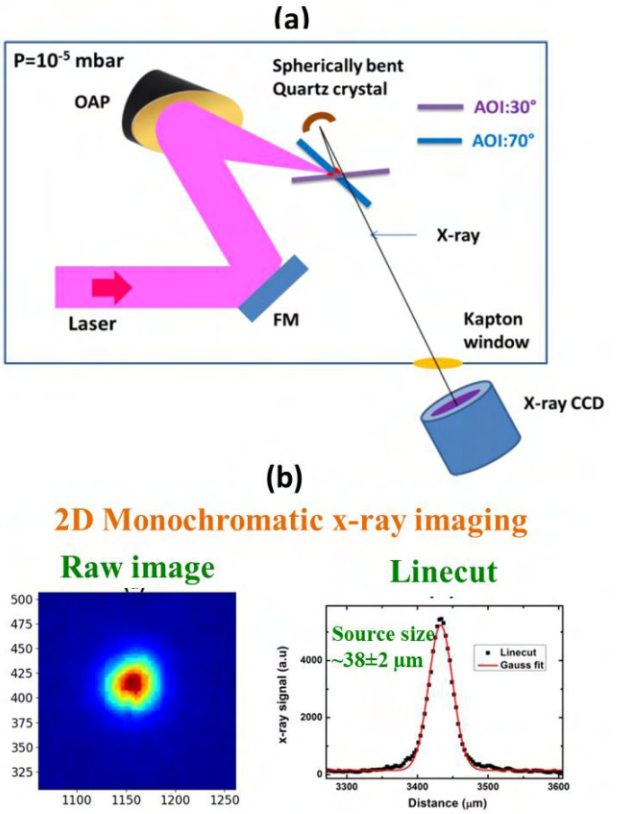

Fig. T.3.10: (a) Experimental setup for monochromatic magnified x-ray imaging for transport studies and (b) raw x-ray images with linecut for source size estimation.

Next, fast electron generation and transport was studied [21] by measuring high resolution Cu K_α lines (Fig. T.3.11) using crystal spectrograph at intensity of ~1x10^{19} W/cm^2 for understanding the generation and refluxing of the electron in subsequent transport through dense matter. Figure T.3.11(a) shows the schematic of the experimental setup for the x-ray measurement. The laser beam of ~30 fs duration was focused by an off-axis parabola (f/ 2.6) on Cu foil at an incidence angle of ~10^0 - 50^0. The intensity on target plane was estimated to be ~1x10^{19} W/cm^2. A cylindrically bent HAPG crystal spectrograph was used to measure high resolution Cu K_α x-ray line emission spectrum in the spectral range of 8.0 – 8.1 keV. Indirect detection x-ray CCD camera was used as detector.

Figure T.3.11(b) shows the spectra of Cu k shell lines containing $K_{\alpha1}$ and $K_{\alpha2}$ for two different polarizations. The conversion of laser energy into K_α radiation increases with the laser intensity as ~$I_L^{0.9}$ and conversion of the order of ~10^{-5} was obtained. The experimentally observed conversion scaling law is in broad agreement with modified model with refluxing considering JxB heating mechanism for fast electron acceleration. The study of x-ray conversion with laser pulse duration demonstrates the role of reacceleration of confined electron after getting reflected from target rear surface. The effect of the transport layer over the target in reducing the sheath field strength was demonstrated. The study with changing the laser polarization shows the signature of the pre-acceleration of electron in the JxB heating by polarization dependent mechanism. The study is useful to identify the parametric regime for increasing the K_α x-ray conversion by maximizing the refluxing efficiency in thin foil target.

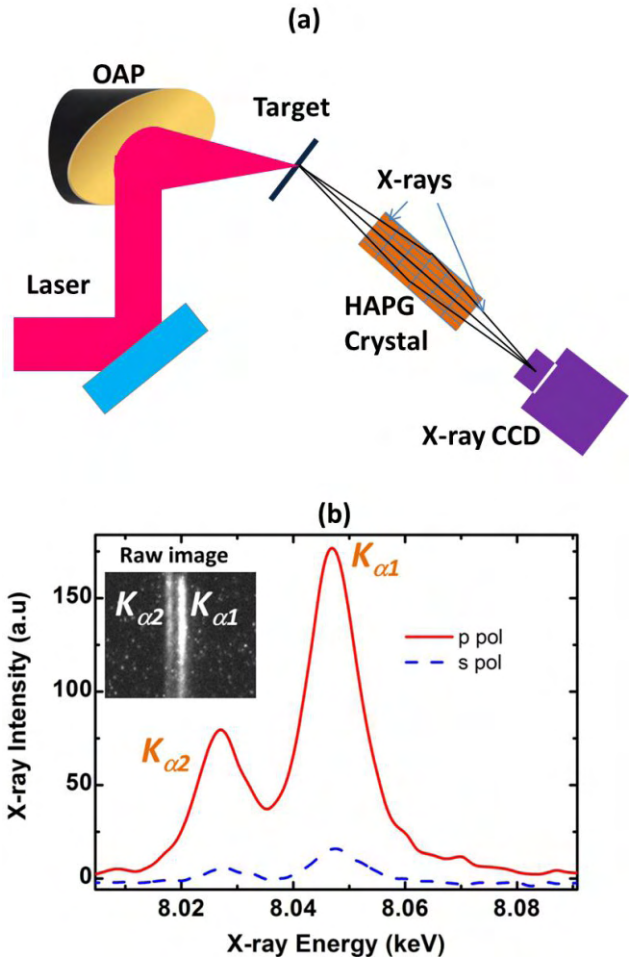

Fig. T.3.11: (a) Experimental setup for high resolution x-ray measurements using HAPG crystal spectrograph and (b) x-ray spectrum from Cu foil for p- and s- polarization at I ~1 x 10^{19} W/cm^2.

7. Conclusion

In conclusion, ultrashort, intense laser plasma interaction was explored through measurement of energetic MeV fast electrons and x-rays. Multiple in-house electron and x-ray diagnostics were developed for the study. The dominance of less explored JxB mechanism was demonstrated in the interaction of ultra-short pulses with foil targets at I~1 - 7x10^{19} W/cm^2. Transverse electron beams along laser polarization direction were found due to ponderomotive scattering. Contrary observation of strong polarization dependence of JxB mechanism was explored and is explained from pre-acceleration in the rising part of laser pulse. The results were supported through detailed PIC simulation, laser absorption and x-ray measurements. Extensive study on electron energy scaling with pre-plasma scale length reveals

that for sharp scale length, electron temperature was lower than the ponderomotive limit whereas for extended scale length, it even produces super-ponderomotive temperature through changes in absorption mechanism in stochastic heating regime. Complex transport phenomena such as refluxing and re-acceleration were clearly demonstrated. Next, electron flux and energy enhancement were obtained using a novel use of simple metallic coated transparent mylar target. Important revelations about the ultrashort rear sheath dynamics was probed by creating a rear plasma using rear metal coating on mylar. Through unique grazing incidence interaction, surface acceleration was demonstrated with high flux and less divergence, which can be a seed for potential practical uses. Finally, the information of refluxed fast electrons confined within the target was obtained through x-ray measurements study, which reveals the important fast electron properties inside target complementing the direct fast electron measurements. The results are very important towards the generation of high charge (nC), high energy (tens of MeV) electron beam, understanding of associated MeV proton beam as well as high flux, hard (keV to MeV) x-ray source for dense plasma and object radiography applications.

Acknowledgement

The present research work has been carried out under the guidance of Dr. A. Moorti, Head, Advanced Plasma Acceleration Section & Laser Electron Acceleration Lab. The author would like to thank Dr. J. A. Chakera, Head, Laser Plasma Division, for valuable suggestions and constant support during the research work. The author sincerely thanks technical advisor Dr. Vipul Arora, for his invaluable advice and suggestions. The author also expresses acknowledgement to Dr. A. Upadhyay for providing PIC simulations support. The author is thankful to Shri R. A. Khan, Shri Ankit, Shri R. A. Joshi and Shri S. Meena for providing laser support and Shri R. P. Kushwaha, Shri S. Sebastin, Shri K. Meena, Shri K. C. Parmar and Shri L. Kisku for providing mechanical support during experiment.

References

[1] P. McKenna, D. Neely, R. Bingham, and D. Jaroszynski, editors, Laser-Plasma Interactions and Applications (Springer International Publishing, 2013).
[2] P. Gibbon, Short Pulse Laser Interactions with Matter (Imperial college press, London, 2005).
[3] D. Strickland and G. Mourou, Opt. Commun. 56, 219 (1985).
[4] M. Tabak et al., Phys. Plasmas 1, 1626 (1994).
[5] A. Macchi, M. Borghesi, and M. Passoni, Rev. Mod. Phys. 85, 751 (2013).
[6] H. Schwoerer et al., Phys. Rev. Lett. 86, 2317 (2001).
[7] S. C. Wilks, W. L. Kruer, M. Tabak, and A. B. Langdon, Phys. Rev. Lett. 69, 1383 (1992).
[8] D. R. Rusby et al., High Power Laser Sci. Eng. 7, (2019).
[9] M. N. Quinn et al., Plasma Phys. Control. Fusion 53, 025007 (2011).
[10] R. J. Gray et al., New J. Phys. 20, 033021 (2018).
[11] H. Chen and S. C. Wilks, Laser Part. Beams 23, 411 (2005).
[12] A. J. Mackinnon et al., Phys. Rev. Lett. 88, 215006 (2002).
[13] A. Yogo et al., Sci. Rep. 7, 1 (2017).
[14] T. Mandal, V. Arora, A. Moorti, A. Upadhyay, and J.A. Chakera, Phys Plasmas 30, 023106 (2023).
[15] T. Mandal et al., Manuscript under preparation (2022). Also presented in 36th PLASMA conference, Dec 13-15, 2021, BIT, Mesra.
[16] T. Mandal, V. Arora, A. Moorti, A. Upadhyay, and J. A. Chakera, Phys. Plasmas 26, 013103 (2019).
[17] T. Mandal, V. Arora, B. S. Rao, A. Moorti, A. Upadhyay, and J. A. Chakera, Phys. Plasmas 26, 043105 (2019).
[18] J. J. MacFarlane et al., J. Quant. Spectrosc. Radiat. Transfer 99, 381–397 (2006).
[19] T. D. Arber et al., Plasma Phys. Controlled Fusion 57, 113001 (2015).
[20] T. Mandal et al., Appl. Phys. B 119, 281 (2015).
[21] T. Mandal, V. Arora, A. Moorti, and J. A. Chakera, Plasma Phys. Control. Fusion, 63, 095009 (2021).